Application of CO2-water-rock reaction transport simulation in NPs-CO2 flooding and storage

Fuping Feng
Northeast Petroleum University
Xu Han (lawliet_hx@163.com)
Northeast Petroleum University https://orcid.org/0000-0002-3410-8138
Shengyuan Liu
Northeast Petroleum University
Dong Jing
China Petroleum Pipeline Engineering Corp
Yanxin Wang
China Petroleum Pipeline Engineering Corp

Research Article

Keywords: CO2 flooding and sequestration, nanoparticles, geochemical reaction, solute transportation

Posted Date: May 13th, 2021

DOI: https://doi.org/10.21203/rs.3.rs-471111/v1

Application of CO_2-water-rock reaction transport simulation in NPs-CO_2 flooding and storage

Fuping Feng [1,2], Xu Han [1,2*], Shengyuan Liu[1,2], Jing Dong[3], Yanxin Wang[3]

[1] Department of Petroleum Engineering, Northeast Petroleum University, Daqing, China.

[2] Key Laboratory of Enhanced Oil Recovery (Northeast Petroleum University), Ministry of Education, Daqing, China.

[3] China Petroleum Pipeline Engineering Corporation, Shanghai, China

* Correspondence: lawliet_hx@163.com; ORCID: 0000-0002-3410-8138;

Abstract: As a hot issue in geological engineering, CO_2 flooding and sequestration still face many challenges. Injection of nanoparticles into CO_2 can improve the injectability and effective reserves of CO_2. However, the migration law of the mixed fluid of CO_2 and nanoparticles (NPs-CO_2) in the reservoir under the condition of chemical reaction is still unclear. Based on chemical reaction kinetics, a mass transfer model of NPs-CO_2 nanofluid in reservoir is established by combining the micro-pore structure change of porous media under CO_2-water-rock reactions condition and the migration law of NPs-CO_2 fluid. The geochemical reaction process between CO_2 and reservoir and the influence of heterogeneity caused by rock microstructure on the miscibility and migration of NPs-CO_2 brine fluid are simulated. The results show that the CO_2-water-rock reaction increases the heterogeneity of reservoir, and the porosity and permeability are rising as a whole; the increase of reservoir heterogeneity caused by chemical reaction can makes the migration of NPs-CO_2 selective. The local accumulation of NPs-CO_2 in the unconnected pores will weaken the original oil displacement efficiency to some extent; in the process of CO_2 sequestration, the density difference between NPs-CO_2 and formation water can not only promote the miscibility of NPs-CO_2-brine fluid, but also inhibit the acid fluid under buoyancy. The upward diffusion is moved to the cover layer to prevent the chemical reaction of the rocks in the cap layer, so as ensuring the permanent storage of greenhouse gases.

Keywords: CO_2 flooding and sequestration; nanoparticles; geochemical reaction; solute transportation

Funding

This work is sponsored by the National Natural Science Foundation, China (No.51774094), China Postdoctoral Science Foundation (2018M641802) and the China Petroleum Science Technology Innovation Fund(2017D-5007-0310). This work is also supported by the “Thirteenth Five-Year Plan” National Science and Technology Major Project (No.2016ZX05016002), Special Postdoctoral Funding in Heilongjiang Province,

China (Postdoctoral Youth Excellence Scheme Lzx-TZ12) and China National Science and Technology Major Project “Changning-Weiyuan shale gas development demonstration project” (2016ZX05062).

Conflicts of interest/Competing interests

The author(s) declare(s) that there is no conflict of interest regarding the publication of this paper.

Availability of data and material

The data used to support the findings of this study are available from the corresponding author upon request.

Code availability

No code were generated during the study.

Authors' contributions

Fuping Feng, Xu Han: Conceptualization; Fuping Feng, Xu Han, Shengyuan Liu: Data curation, Writing-Original draft preparation; Shengyuan Liu, Jing Dong, Yanxin Wang: Visualization, Investigation; Fuping Feng, Xu Han: Supervision; Xu Han: Methodology, Software, Validation; Xu Han: Writing- Reviewing and Editing

1. Introduction

Since the successful implementation of CO_2 flooding and storage project in 1972 in the United States, nearly 140 related projects have been large-scale implemented in oil fields around the world (Bergmann et al. 2016; Hu et al. 2019). It has been proved that CO_2 flooding, as a kind of gas flooding, can improve the fluid properties of the reservoir, extract the oil and gas resources stored in the pores and micro fractures, and greatly improve the oil recovery (Emberley et al. 2004). Meanwhile, Carbon Capture and Storage (CCS) is the best way to achieve greenhouse gas emission reduction under the current economic and technological conditions (Huang et al. 2016). However, after CO_2 injection, some undissolved fluids in formation water will move upward and diffuse under the action of buoyancy, which not only reduces the oil displacement efficiency, but also has the risk of leakage (Zhang et al. 2014).

Aiming at these problems, Farzam et al. (2011) proposed for the first time that a kind of nanoparticles should be added into injected CO_2. Depleted uranium can be generated as a very small volume of nanoparticles. When CO_2 is added for treatment, it will form a nonreactive mixture which can increase the density of storage fluid, shorten the mixing time, reduce the buoyancy, and make CO_2 safely sealed in the reservoir. Furthermore, they can be added to CO_2 used in oil fields to form a homogeneous dispersion system, which has become a new technology for EOR in recent years (Zhan et al. 2016; Hendraningrat et al. 2013; Wang 2018; Guo and Aryana 2016; Prigiobbe et al. 2016; Yang et al. 2014). The above results show that CO_2-nanofluid can not only improve oil displacement efficiency, but also increase the safety of greenhouse gas storage. It is worth noting that no

CO_2-water-rock reactions have been considered in the above studies. However, the common calcite, feldspar, quartz, and clay minerals in reservoir can react with CO_2 in a complex way (Ahmad et al. 2016; Jung et al. 2013; Mohammad et al. 2015; Iglauer et al. 2015; Andrew et al. 2014; Harpreet et al. 2012; Rathnaweera et al. 2016; Lasaga et al. 1994; Plummer and Busenberg 1999; Ranganathan et al. 2011; Rosenbauer et al. 2012; Daval et al. 2013; Ward et al. 2014). With long-term CO_2 flooding/seal process possible mineral composition, the change of pore structure, porosity and permeability, the migration law of NPs-CO_2 is unclear, likewise, in under the action of water rock reaction should not be neglected, NPs-CO_2 flooding effect and reflected in the safety of the storage advantage may deviate from the original thought.

In order to clarify the migration rule of NPs-CO_2 under CO_2-water-rock reactions and its influence on oil displacement/geological sequestration project, the chemical reaction equilibrium equation is used to quantify the physical property changes such as porosity and permeability of reservoir, and the mass transfer model of NPs-CO_2-brine system is established based on the percolation equation. The geochemical reaction process of shale reservoir after NPs-CO_2 fluid injection is simulated, and the influence of rock microstructure changes on the miscibility and migration of NPs-CO_2-brine fluid is reached. According to the previous similar studies on NPs-CO_2, CO_2 will form a non-reactive stable mixture with NPs and will not participate in chemical reaction under formation conditions, so the chemical properties of nanoparticles were not considered in this study.

2. Theory and Modeling

2.1. Theoretical description

For the percolation process including the chemical reactions of heterogeneous porous media, the flow pattern is determined by the density difference between the mixed fluids, the reaction rate of the fluid and the change of the porous media porosity. That is to say, after NPs-CO_2-brine injection into the formation, the solvent moves to the lower part of the reservoir, and dissolution or precipitation reactions occur between solvent and formation rock particles, resulting in the porosity and permeability of the reservoir changes. The injected fluid is easier to flow down driven by the density difference, when the fluid flows from the area with large permeability to the area with small permeability, there is a small disturbance at the front edge, and the amplitude of the disturbance will increase with time, forming an unstable flow pattern of reactive and transport (Chadam et al. 1986; Chadam et al. 1991), and the rock matrix are further dissolved, these three processes promote and couple with each other, which further increases the instability at the interface.

88 *2.1.1. Chemical reaction kinetics*

89 When ions migrate to the surface of minerals, they react with minerals, dissolve to form free ions, or
90 precipitate to form secondary minerals. According to the chemical kinetics law, for a series of solid-liquid
91 surface reactions, the mineral reaction rate can be expressed as follows (Bethke 1996):

92
$$\mathrm{R}_{\beta} = \hat{\mathrm{A}}_{\beta} k_{\beta} \left(1 - \frac{\mathrm{Q}}{K_{eq,\beta}} \right), \beta = 1, ..., \zeta_{\mathrm{mn}} \tag{1}$$

93 Where, ζ_{mn} is the amount of reactions; $\mathbf{R}_{\beta}$ is the velocity of reactions, mol/L·s^{-1}; A is the reactive surface
94 area of mineral, m^2 ; k_{β} is the reaction rate constant; K_{eq} is the equilibrium constant of reaction, Kharaka
95 (1992) listed the numerical value of K_{eq} as a function of temperature; $\frac{\mathrm{Q}}{K_{eq,\beta}}$ is the saturation index of the
96 reaction, if $\frac{\mathrm{Q}}{K_{eq,\beta}}$<1, mineral dissolution occurs, Otherwise mineral precipitation occurs; Q is an activity
97 product [30]:

98
$$\mathrm{Q}_{\beta} = \prod_{k=1}^{\mathrm{n_{aq}}} \mathrm{a}_k^{\nu_{k\beta}} \tag{2}$$

99 Where, $\mathbf{n}_{\mathrm{aq}}$ is the number of ions in the solution, a_k is the activity of the reactive component, $\boldsymbol{\nu}_{k\beta}$ is the
100 stoichiometric coefficient of equilibrium reaction, the stoichiometric coefficient of reactants is negative, and
101 product is positive.

102 *2.1.2 Material transport equilibrium*

103 After NPs-CO_2 injection into the reservoir, convection and diffusion occur. Convection is the migration
104 process of ions in solution flowing with pore water. The process of fluid flow and miscibility driven by density
105 difference in porous media can be expressed as follows:

106
$$\phi \frac{\partial \rho_l}{\partial t} + \frac{\partial \left(\rho_l u_x \right)}{\partial x} + \frac{\partial \left(\rho_l u_z \right)}{\partial z} = 0 \tag{3}$$

107 Where, ϕ is porosity; ρ_l is the density of liquid, kg/m^3; u_x (u_z) is the velocity along x-axis(z-axis), m/s; t is
108 time, s.

Darcy's law (Cardoso and Andres 2014):

$$u=-\frac{k}{\mu}\left(\nabla p-\Delta\rho g z\right) \tag{4}$$

Where, k is permeability, m^2; μ is the viscosity, $kg/m\cdot s^{-1}$; p is pressure, Pa; g is gravitational acceleration, m/s^2.

Density (Smith et al. 2005) and viscosity (Kim et al. 2004) of mixed fluid:

$$\frac{\rho_{\text{NPs-CO}_2\text{-brine}}}{\rho_{\text{CO}_2\text{-brine}}}=\left(1-f\right)+f\frac{\rho_{\text{NPs}}}{\rho_{\text{CO}_2\text{-brine}}} \tag{5}$$

$$\frac{\mu_{\text{NPs-CO}_2\text{-brine}}}{\mu_{\text{CO}_2\text{-brine}}}=\frac{1}{\left(1-f\right)^{2.5}} \tag{6}$$

Where, *f* is volume fraction of NPs to that of base fluid; NPs are nanoparticles; CO_2-brine is brine saturated with CO_2; NPs-CO_2-brine is brine saturated with NPs and CO_2.

The transport and chemical reaction processes of ions in solution follows the law of mass conservation (Zhang et al. 2016), that is to say the decrease of solute concentration in any unit is equal to the sum of convection, diffusion and reactions, and the ions diffuse from high concentration area to low concentration area, and finally tend to balance. The equation of mass transport equilibrium can be obtained by combining the diffusion phenomenon caused by the change of concentration gradient with flow and chemical reactions, according to the mass conservation principle of each ion concentration in chemical solution passing through any unit of porous media. The change of substance concentration in porous media includes three parts on the right side of the equation. The first term on the right side of the equation is the change of substance diffusion, the second term is the change of flow and migration, and the third term is the change of water-rock reactions.

$$\frac{\partial\left(\phi C_i\right)}{\partial t}=\nabla\cdot\left(\phi D_i\nabla C_i\right)-\nabla\cdot\left(uC_i\right)-\sum_{\beta=1}^{N_\beta}v_{i\beta}R_\beta \tag{7}$$

Where, C_i is the concentration of material *i* mol/m^3; D is diffusion coefficient, m^2/s; $\nu_{i\beta}$ is the stoichiometric coefficient of material i in equilibrium reaction β.

2.2.3 Initial and boundary conditions

The initial saturation of NPs-CO_2 solution in the reservoir was set to 0, only considering the inflow of fluid. The whole reaction process was carried out in a closed environment without mass exchange. The concentration of ions in the initial formation water was evenly distributed in the grid, they changed with the time of chemical reaction, which was subject to the chemical rate equation of water-rock reaction.

$$Sg_{\mathrm{CO_2}}(t)\big|_{\partial t} = 0 \tag{11}$$

$$C_i(x, y, z)\big|_{t=0} = C_0 \tag{12}$$

$$C_i(t)\big|_{\partial\Omega} = C_0 - R_{\mathrm{m}} \tag{13}$$

2.1.3 Changes of rock microscopic physical properties

According to the chemical equilibrium equation, the change quantity of a certain mineral quality participating in chemical reaction in reservoir rock can be obtained:

$$\frac{\partial m}{\partial t} = \frac{\partial(n \cdot M)}{\partial t} = \frac{\partial(\rho V \cdot \phi)}{\partial t} \tag{8}$$

Where, m is the quality of a substance participating in a chemical reaction, g; M is the molar mass of the mineral component, mol/g; V is the molar volume of the mineral component, mol/cm^3; n is the amount of mineral substance participating in the chemical reaction, mol.

There are many kinds of minerals in the reservoir rock that have chemical reaction at the same time, the pore volume reduction of various minerals participating in chemical reaction in the reservoir rock can be superposed and simplified as follows:

$$\frac{\partial \phi}{\partial t} = \frac{1}{V} \cdot \sum \frac{\partial n_i}{\partial t} \cdot \frac{M_i}{\rho_i} \tag{9}$$

The change of matrix permeability of a single rock reference unit can be calculated by the change of porosity. The change of permeability with porosity is calculated according to Carman-Kozeny formula (Xu et al. 2014; Xu et al. 2012):

$$k = k_0 \frac{(1-\phi_0)^2}{(1-\phi)^2} \left(\frac{\phi}{\phi_0}\right)^3 \tag{10}$$

Where, ϕ, ϕ_0 are the porosity of rocks in the grid after and before the reaction respectively; k, k_0 are the permeability of rocks in the grid after and before the reaction respectively, m^2.

2.2 Model description

The numerical simulation model was established in the mainly refers to the actual situation of the typical CO_2 buried block, which is a three-dimensional saturated formation water area, and the height and length of the model are H and L respectively (Fig.1). Geochemical reaction process was used to quantify the microstructure change of shale reservoir, and the vertical and horizontal diffusion processes of CO_2 fluid from injection point with the increase of formation heterogeneity were discussed. The flow field and concentration field of groundwater under the condition of steady flow are used as the initial conditions of the unsteady flow model. The lateral boundary near the injection point is set as symmetry, the upper and lower part of the reservoir is set as impermeable boundary, and the lateral boundary of the far well formation is set as outflow boundary.

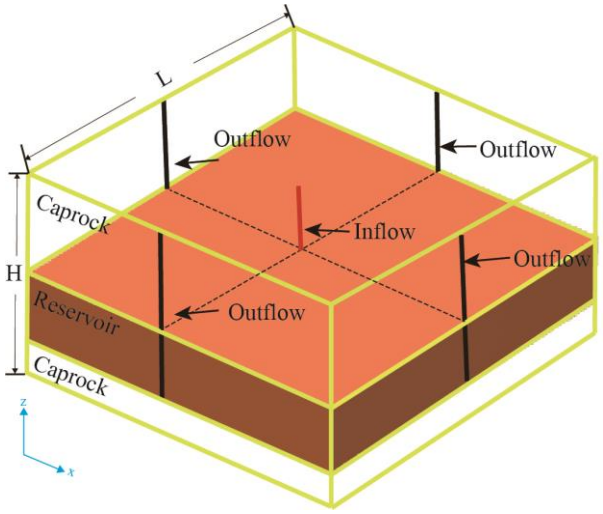

Figure 1. Three-dimensional stratigraphic model

2.2.1 Model assumption

(1). There was no adsorption on the surface of the reservoir;

(2). The chemical reactions all take place under isothermal condition;

(3). The minerals in the reservoir are evenly distributed, and the physical properties conform to their initial porosity and permeability;

(4). The inhibition of convection caused by the consumption of CO_2 in chemical reactions is ignored;

(5). The nano particles are uniformly dispersed in CO_2, which will not agglomerate or precipitate due to the consumption of CO_2 in chemical reactions.

174 *2.2.2 Parameters used in the simulation*

175 Table 1 shows the initial data set generally applicable to CO_2 storage.

176 Table 1. Reservoir Parameters

Thickness /m	Density / kg·m^3	Average Porosity	Average Permeability /mD
190~280	2500	0.12	0.15
The ratio of horizontal to vertical permeability	Average temperature /°C	Median pore radius/μm	Pressure /MPa
10	100	0.1	25

177 Initial mineral content of reservoir is consulted with the potential saline aquifers in North America which

178 are suitable for the storage of CO_2 (Zhang et al. 2015).

179 Table 2. Initial parameters used in chemical reaction model

Initial mineral content of reservoir /%						
Quartz	Oligoclase	Calcite	K-feldspar	Kaolinite	Chlorite	Smectite-Na
59.181	10.662	1.929	8.179	2.015	10.031	8.003
Initial composition of formation water /mol·kg^{-1} H_2O						
H^+	0.432×10^{-1}	Na^+	0.989	Fe^{2+}	0.302×10^{-6}	K^+	0.596×10^{-2}
SiO_2	0.103×10^{-2}	HCO_3^-	0.456×10^{-1}	Ca^{2+}	0.473×10^{-2}	Mg^{2+}	0.267×10^{-4}

Reaction equation (Yu 2015; Mangold and Tsang 1999; Busenberg and Plummer 2011)	A (Zhang et al. 2015)	Log Keq (Palandri et al. 2004)
Quartz $\Leftrightarrow$ SiO_2(aq)	9.8×10^{-4}	-9.36
Oligoclase+H_2O+CO_2+2Na^+ $\Leftrightarrow$ 2Dawsonite+Ca^{2+}+6SiO_2	9.8×10^{-4}	-11.63
Calcite+H_2O+CO_2 $\Leftrightarrow$ Ca^{2+}+2HCO_3^-	9.8×10^{-4}	-0.30
K-Feldspar+2H^++9H_2O $\Longrightarrow$ 2K^++4H4SiO4+Kaolinite	9.8×10^{-4}	-5.76
Kaolinite+6H^+ $\Longrightarrow$ H_2O+2Al^{3+}+2SiO2(aq)	151.6×10^{-4}	-11.31

$Chlorite+2.5Ca^{2+}+5CO_2+1.5H_2O \Longrightarrow Ankerite+Kaolinite+Mg^{2+}+3H^+$	9.8×10^{-4}	-11.11
$Albite+CO_2+H_2O \Leftrightarrow Dawsonite+3SiO2$	9.8×10^{-4}	-9.87
$Smectite\text{-}Na+6K^++2H_2O \Leftrightarrow Kaolinite+2Na^++Mg^{2+}+2H^++Si(OH)_4$	151.6×10^{-4}	-10.98

3. Results and discussion

3.1 Change of each mineral content

The chemical reaction process was shown in Table 2 and the simulation time is 100 years.

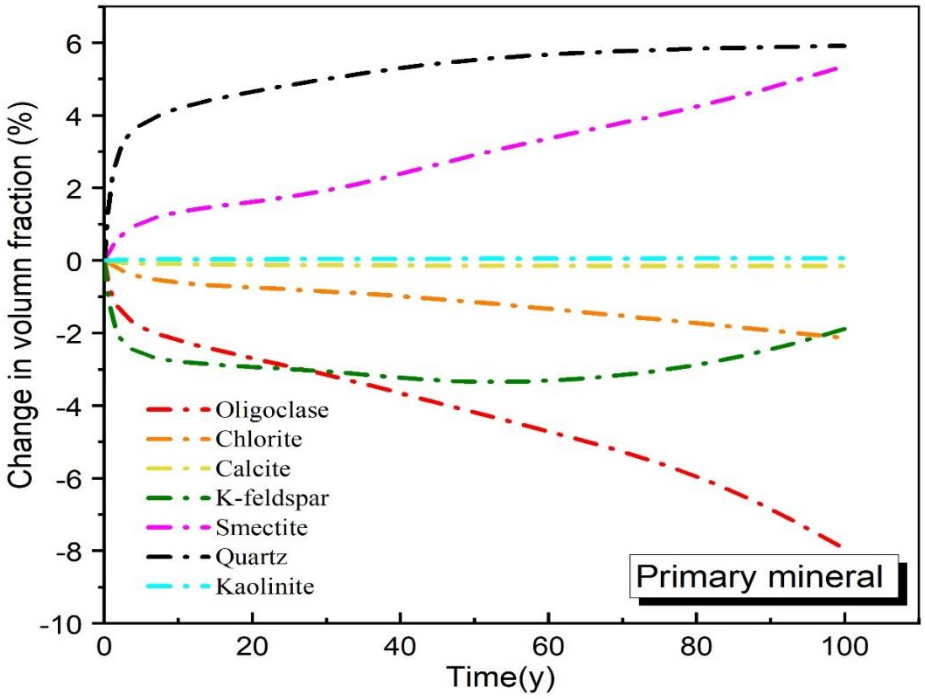

(**a**) **Primary mineral**

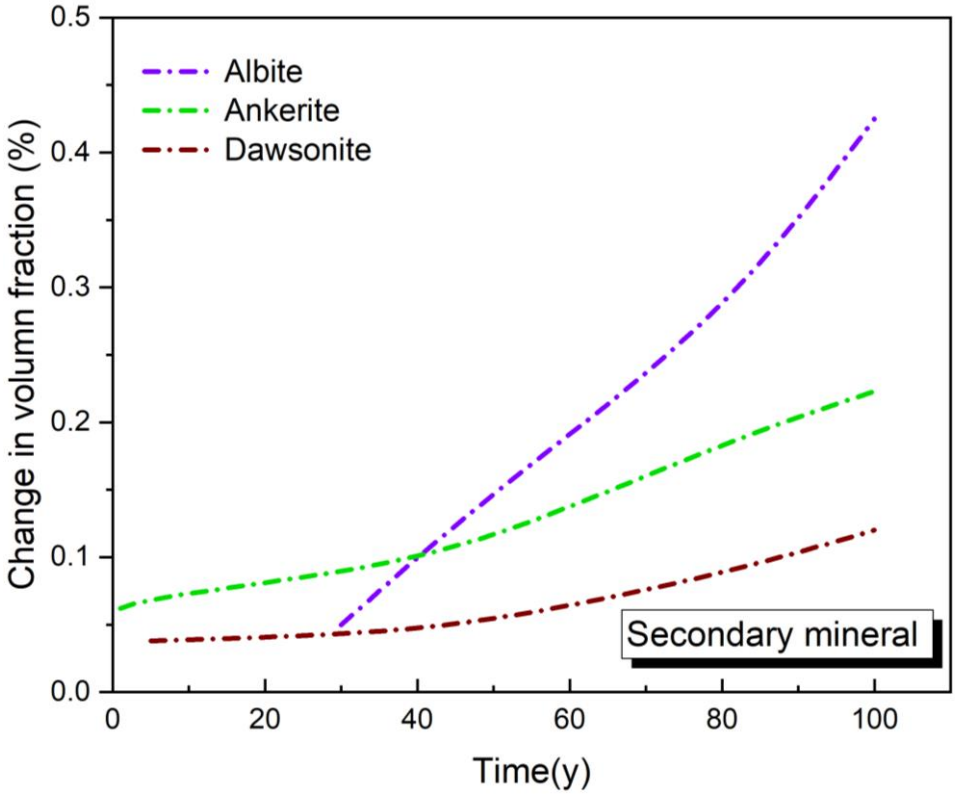

(**b**) **Secondary mineral**

Figure 2. Volume fraction changes of minerals

In the simulation process, the minerals that have the dissolution reactions are oligoclase, chlorite, calcite and K-feldspar; the minerals with precipitation reactions are smectite, quartz and kaolinite. In addition to the above minerals, there are three kinds of secondary minerals. The generation is ankerite, dawsonite and albite.

The results showed that the dissolution of oligoclase and K-feldspar mainly provides Ca^{2+} and K^{+} for formation of aqueous solution. SiO_2, Al^{3+} and Na^{+} formed by the dissolution reactions of feldspar contributed to the precipitation reactions of montmorillonite and the formation of albite and dawsonite in the later stage, while the dissolution of chlorite also provided enough cations for ankerite. Quartz was affected by the process of dissolution and precipitation. The solid particles on the surface of quartz dissolve in formation water could form a solution, while the precipitation was due to the SiO_2 which was produced by the dissolution of primary minerals, which made quartz in formation water saturated and precipitated. Although the change degree of mineral volume fraction varied in about 100 years, the amount of mineral dissolution was always greater than that of precipitation.

The change of mineral content in reference (Zhang et al. 2015) can verify the correctness of this chemical reaction model. Different from Zhang (2015), Different from Zhang (2015), the effect of density difference of

carbonate fluid formed after CO_2 dissolution on solute diffusion and the heterogeneity of formation porosity and permeability after chemical reaction were additionally considered in this paper, which would be further discussed below.

3.2 Porosity, permeability and heterogeneity

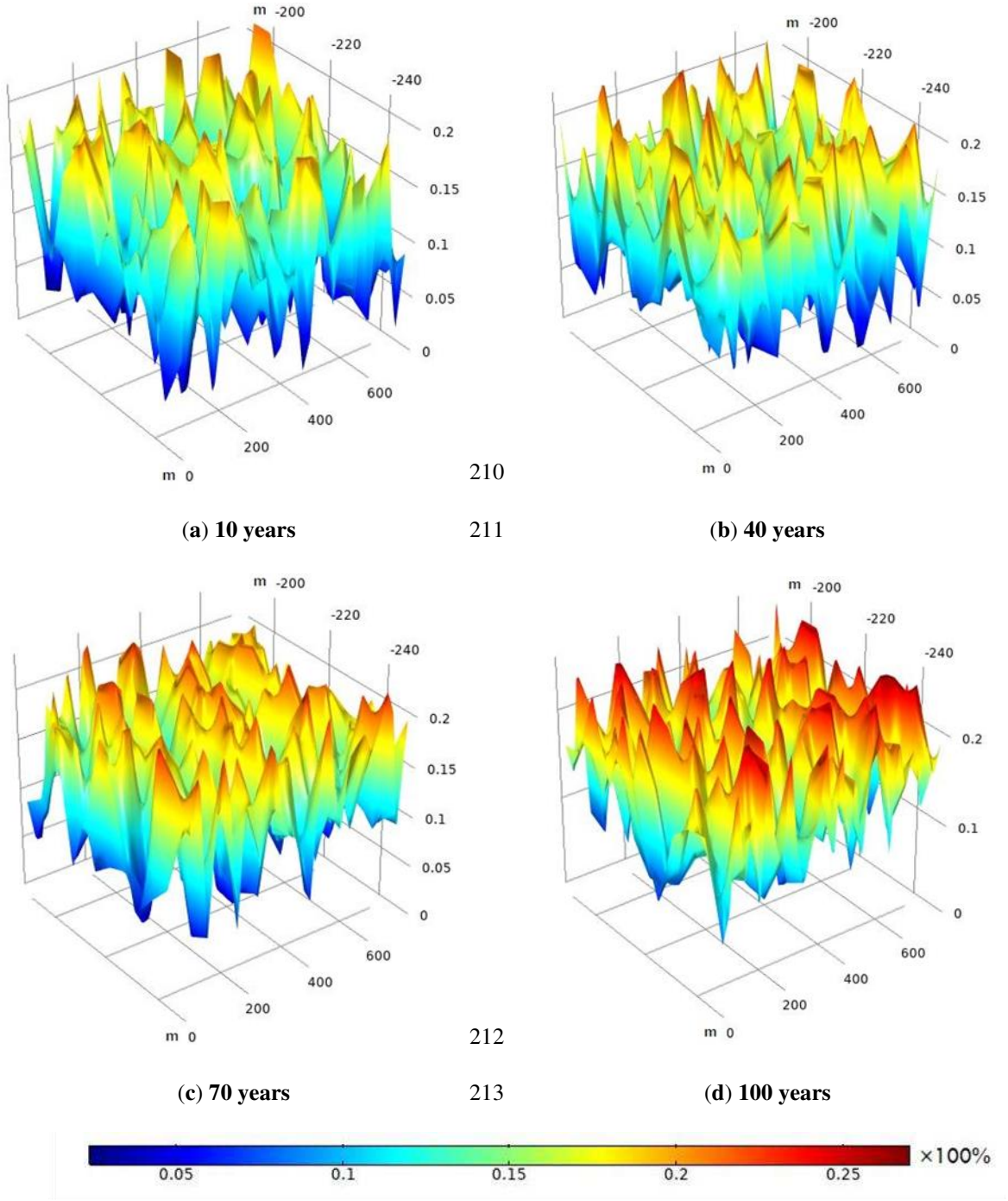

Figure 3. Change of reservoir porosity

During 100 years of simulated chemical reaction process, the porosity of different reservoir locations had increased or decreased, which was attributed to the dissolution and precipitation reaction of different minerals. The porosity range changed from 2.40% to 21.58% after 10 years of injection (Fig.3a), from 3.34% to 22.20% after 40 years (Fig.3b), from 4.55% to 23.50% after 70 years (Fig.3c), and from 6.43% to 25.84% after 100 years (Fig.3d). However, the physical properties of the reservoir are improved, the average porosity increased from 12% to 16%, indicating that the dissolution reaction played an important role after CO_2 injection.

The permeability of reservoir can be regarded as the concentrated expression of reservoir heterogeneity. Therefore, in order to describe the change process of reservoir heterogeneity more intuitively, in the study of formation rock permeability, the injection layer section at Y(700m)-Z(90m) section is taken as the research object (Fig.4).

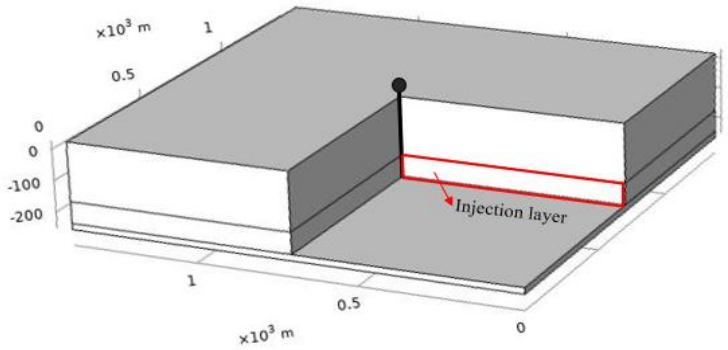

Figure 4. Schematic diagram of injection layer model section

The simulation result of permeability change with time at the reservoir section is shown as Figure 5.

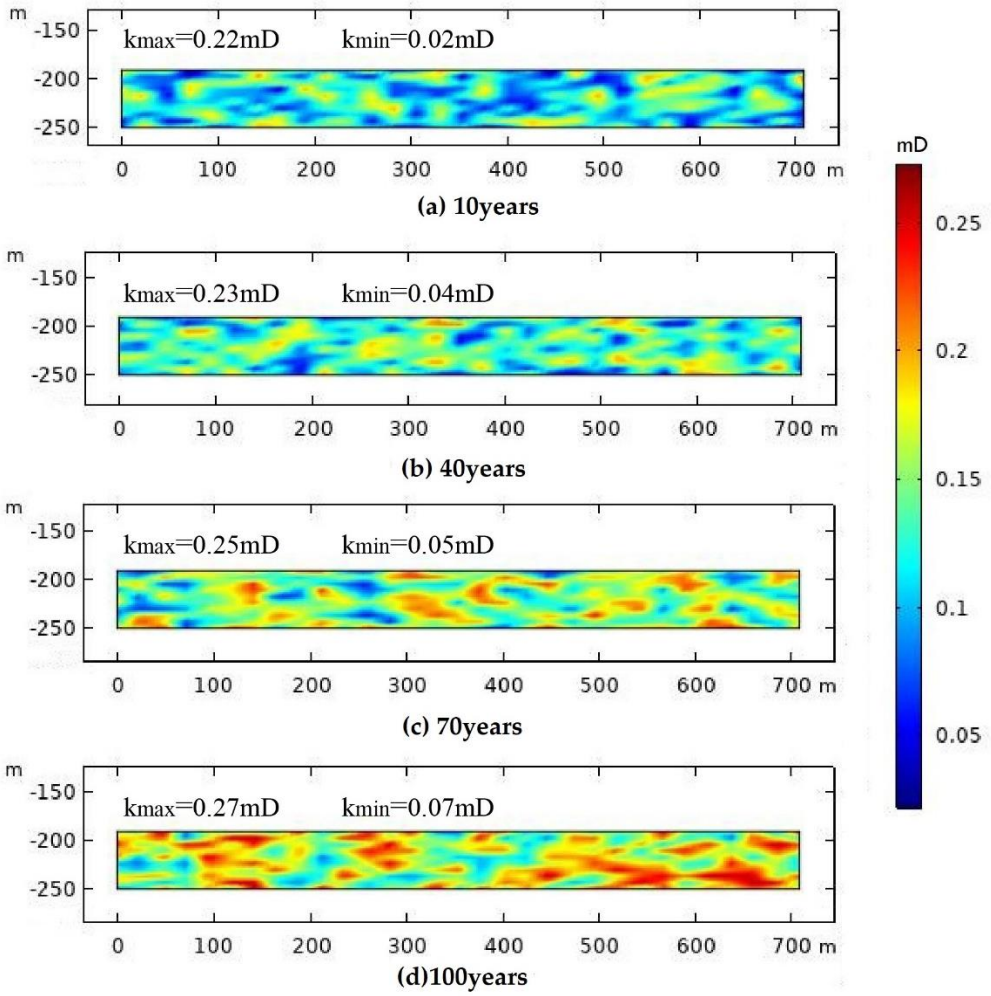

Figure 5. Change of reservoir permeability

The change rule of permeability at different reservoir locations was directly proportional to porosity. The permeability range changed between 0.02~0.22mD after 10 years of injection(Fig.5a), between 0.04~0.23mD after 40 years(Fig.5b), 0.05~ 0.25mD after 70 years (Fig.5c), and from 0.07~0.27mD after 100 years (Fig.5d). The average permeability increased from 0.013 mD to 0.017 mD.

In this study, Lorenz coefficient (Fitch et al. 2010) is introduced as the calculation method of permeability variation coefficient (see Appendix A).

The permeability variation coefficient at the injection section changes with time as shown in Figure 6.

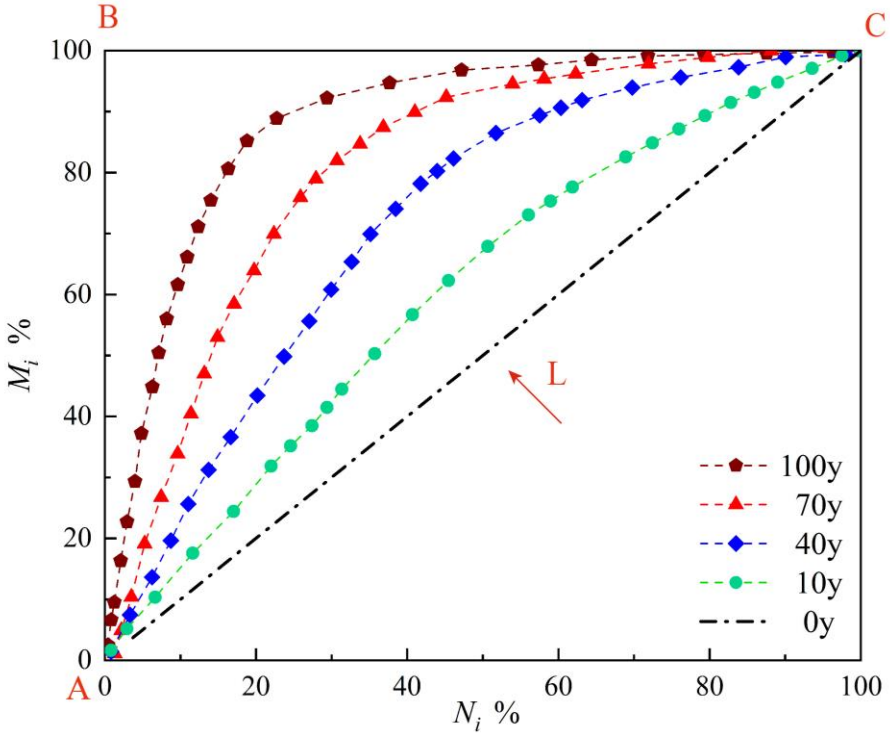

Figure 6. Lorentz curve of rock heterogeneity

With the increase time of chemical reactions, the heterogeneity of the injection layer increased gradually. This is because the dissolved minerals increase the pore throat radius of the reservoir, while the precipitated mineral particles will adhere to the pore throat or flow with the fluid, blocking the small pores, changing the permeability at different positions, and then CO_2-water-rock reaction affects the migration path and path size of fluid by changing the micro-structure of rock.

3.3 Fluid flow and mixing

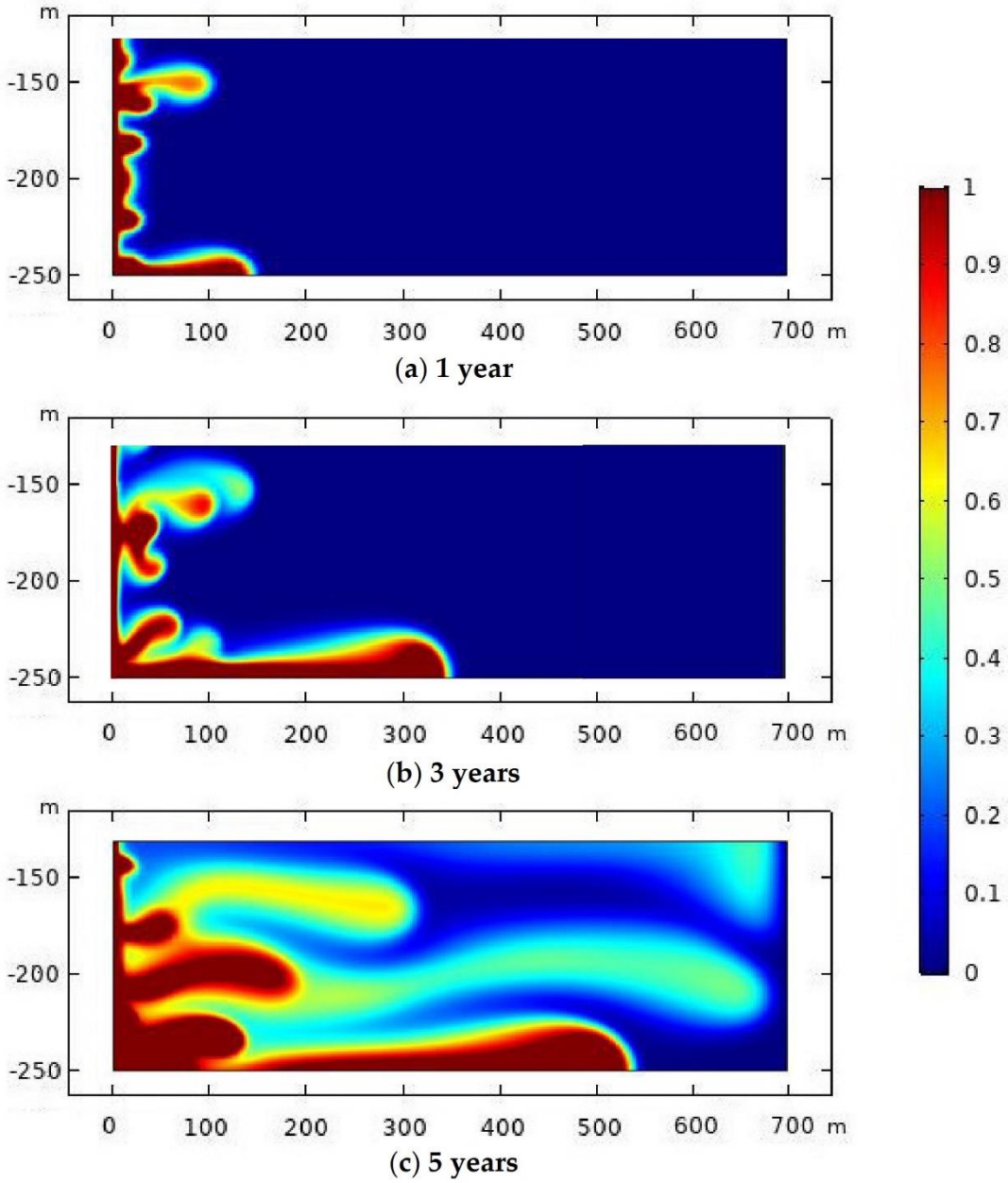

Figure 8. Change of NPs-CO_2 saturation after chemical reactions

As the density of NPs-CO_2 is slightly higher than the formation water. After injection (Fig.8), it moved downward under the action of gravity overcoming buoyancy and spread along the horizontal direction. Because of the density difference of miscible fluid, the miscible interface did not move forward as a flat interface under the action of gravity, but developed into a fingerlike shape, namely, Rayleigh Taylor instability. With the increasing mixing of NPs-CO_2-brine, the density difference at the front edge was decreasing, which weakened the downward movement of fluid front interface. This phenomenon of slowing down CO_2 fingering can achieve the expected stable displacement of CO_2. However, with the development of chemical reaction, the pore structure of reservoir rock changes, and the dissolved solid part is more likely to form a fluid flow channel. This

effect and the Rayleigh Taylor instability caused by density difference superimposed, which further leads to the instability of the interface.

3.4 Velocity of flow

In order to reduce the iteration times and internal degrees of freedom, a 500 × 1000 μm rectangle near the injection point (x = 0 ~ 500 μm, z = 0 ~ 1000 μm) is selected as the research object. The rock matrix of rock before reaction was assumed to be uniformly distributed, the porosity difference before and after the reaction was calculated, and the data (i.e. the secondary minerals formed by precipitation reaction) at the position with the difference less than 0 is eliminated (Figure 9), Based on the new geometric model, the numerical simulation of fluid flow is established (Figure 10).

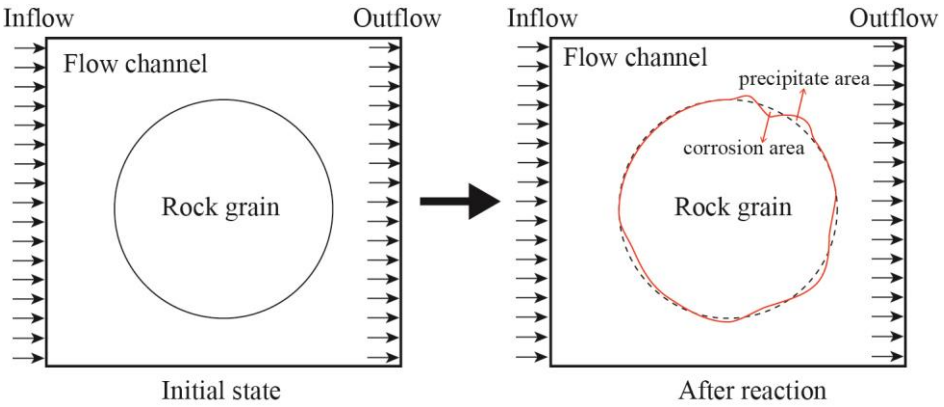

Figure 9. Geometric model after microstructure change

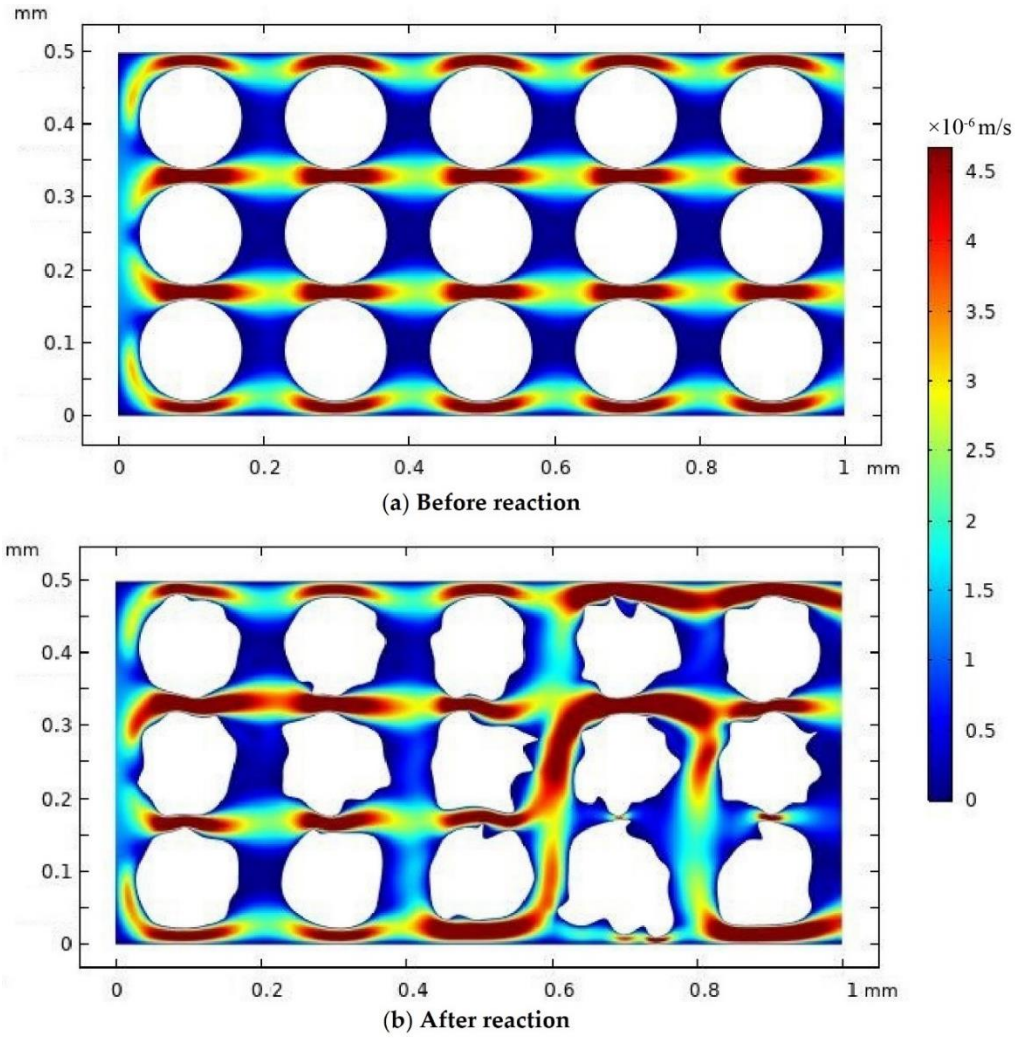

Figure 10. Velocity change of NPs-CO_2 flow

With the increase of formation heterogeneity, the microstructure of rocks in different positions also changes correspondingly, which shows that the primary mineral dissolution area appears to depression, and some positions appear to bulge due to attached secondary mineral precipitation. The heterogeneity of rock increases and the fluid flow path changes. In other words, the smaller the cross-sectional area of the fluid channel is, the greater the velocity is, which promotes the selective migration of NPs-CO_2. After the chemical reaction, the roughness around the rock skeleton increases obviously, and the fluid velocity in the rock depression is close to 0, which means the local accumulation of NPs-CO_2. The local velocity fluctuation of fluid can improve the mixing time and degree of NPs-CO_2 with formation water.

Therefore, after considering the influence of geochemical reaction, different conclusions appear in the process of oil displacement and carbon sequestration. In the process of oil displacement, the change of micro pore fine structure makes the migration of NPs-CO_2 selective, the local accumulation of NPs-CO_2 in the unconnected pores weakens the original oil displacement efficiency to some extent; In the process of CO_2

sequestration, the density difference between NPs-CO_2 and formation water can not only promote the miscibility of NPs-CO_2-brine fluid, but also inhibit the acid fluid under buoyancy. The upward diffusion is moved to the cover layer to prevent the chemical reaction of the rocks in the cap layer, to ensure the permanent storage of greenhouse gases.

4. Conclusions

In this paper, the chemical reaction and fluid flow model of NPs-CO_2 fluid injected into shale reservoir are established, the mechanism of CO_2-water-rock reaction, the law of mineral transformation and rock physical property evolution are revealed, and the law of NPs-CO_2 fluid reaction and migration under the condition of heterogeneous reservoir is obtained. Through this work, three important conclusions can be drawn, which are:

(1) The primary mineral composition of the reservoir is the key factor affecting the CO_2-water-rock reaction. The micro mechanism of the reaction and the change of pore structure directly affect the overall efficiency of CO_2 flooding and storage. The simulated formation rock dissolution reaction and precipitation reaction are carried out at the same time, and three kinds of secondary minerals are generated in the first 30 years of simulation. With the extension of chemical reaction time, the sedimentation rate gradually increases, but the average porosity and permeability show an overall upward trend, indicating that the mineral dissolution amount is always greater than the precipitation amount, and the reservoir physical properties are improved.

(2) In the process of oil displacement, the change of rock microstructure caused by CO_2-water-rock reaction will have a negative impact on fluid migration. The location of secondary mineral precipitation will narrow the fluid migration channel, and then block up. The corrosion pit will cause the local accumulation of solute, making the fluid migration rate close to 0, resulting in the failure of NPs-CO_2 mixed fluid to achieve the expected oil displacement efficiency.

(3) In the process of storage, the enhancement of reservoir heterogeneity caused by chemical reaction and the improvement of physical properties can improve the local velocity fluctuation and miscibility degree of nanofluids, and by increasing the density of mixed fluids, most acidic fluids are located at the bottom of the reservoir and diffuse along the horizontal direction, which is more conducive to the safe storage of CO_2.

Conflicts of Interest: The authors declare no conflict of interest.

Appendix A

In the Lorentz curve drawn, the actual cumulative permeability distribution curve is between AC and BC, showing a convex curve L. The more the curve L deviates from AC, the more serious the heterogeneity is.

The specific calculation method is as follows (Li 2006).

(1) Calculate the relative permeability contribution percentage of each unit rock:

$$W_i = \frac{K_i}{\sum_{i=1}^{n} K_i} \times 100 \tag{14}$$

Where, W_i is the permeability contribution value of unit i, %; K_i is the permeability of unit i, $10^{-3}\mu m^2$; n is the total number of permeability units in the target layer.

(2) Calculate the cumulative permeability contribution of sample k:

$$M_i = \sum_{i=1}^{k} W_i \qquad k \in (1, 2, 3, ..., n) \tag{15}$$

(3) Calculate the cumulative percentage of each rock sample:

$$Q_i = \frac{P_i}{\sum_{i=1}^{n} P_i} \times 100 \tag{16}$$

$$N_i = \sum_{i=1}^{k} Q_i \tag{17}$$

Where, Q_i is the percentage of sample i, %; P_i is the unit number of sample i; N_i is cumulative percentage of rock sample corresponding to sample i, %.

References

1. Andrew J. Worthen, Parth S. Parikh, Chen Y, et al (2014) Johnston. Carbon Dioxide-in-Water Foams Stabilized with a Mixture of Nanoparticles and Surfactant for CO_2 Storage and Utilization Applications. Energy Procedia 63:7929-7938.
2. Bergmann. P, Diersch. M, Götz. J, Ivandic. M et al (2016) Review on geophysical monitoring of CO_2 injection at Ketzin, Germany. Journal of Petroleum Science and Engineering 139: 112-136.
3. Bethke C M (1996) Geochemical reaction modeling: concepts and applications. Oxford University Press 53(2):205-214.
4. Busenberg E and Plummer L N (1982) The kinetics of dissolution of dolomite in CO_2-H_2O systems at 1.5 to 65°C and 0 to 1atm PCO_2. American Journal of Science 282:45-78.

5. Cardoso S S S and Andres J T H (2014) Geochemistry of silicate-rich rocks can curtail spreading of carbon dioxide in subsurface aquifers. Nature Communications 5:5743.

6. Chadam J., Hoff D., Merino E., et al. Reactive infiltration instabilities. IMA J. Appl. Math.， 1986, 36:207-221

7. Chadam, J. and Ortoleva, P (1988) Reaction-infiltration instabilities. Numerical simulation in oil recovery 11:67–76.

8. Chadam J., Peirce A., Ortoleva P (1991) Stability of reactive flows in porous media: coupled porosity and viscosity changes. Siam Journal on Applied Mathematics 51:684-692.

9. Daval D, Hellmann R, Martinez I, et al (2013) Lizardite serpentine dissolution kinetics as a function of pH and temperature, including effects of elevated pCO_2. Chemical Geology 351:245-256.

10. Emberley. S, I. Hutcheon. I, Shevalier. M et al (2004) Geochemical monitoring of fluid-rock interaction and CO_2 storage at the Weyburn CO_2-injection enhanced oil recovery site, Saskatchewan, Canada. Energy 29(9-10):1393-1401.

11. Fitch Peter, Davies Sarah, Lovell Mike, Pritchard Tim, Sirju Clive (2010) Heterogeneity In Carbonate Petrophysical Properties: Application to Fluid Flow Units And Sampling Strategies. Society of Petrophysicists and Well-Log Analysts, SPWLA-2010-92910.

12. Guo F and Aryana S (2016) An experimental investigation of nanoparticle-stabilized CO_2 foam used in enhanced oil recovery. Fuel 186(dec.15):430-442.

13. Hendraningrat L, Li S, Toraseter O (2013) A coreflood investigation of nanofluid enhanced oil recovery. Journal of Petroleum Science and Engineering 111:128-138.

14. Hu Y, Hao M, Chen G, et al (2019) Technologies and practice of CO_2 flooding and sequestration in China. Petroleum Exploration and Developmen 46(4): 1-12.

15. Huang F, Huang H, Wang Y, et al (2016) Assessment of miscibility effect for CO_2 flooding EOR in a low permeability reservoir. Journal of Petroleum Science and Engineering 145:328-335.

16. Iglauer S, Pentland C H, Busch A (2015) CO_2 wettability of seal and reservoir rocks and the implications for carbon geo-sequestration. Water Resources Research 51(1):729-774.

17. Javadpour F and Nicot J P (2011) Enhanced CO_2 Storage and Sequestration in Deep Saline Aquifers by Nanoparticles: Commingled Disposal of Depleted Uranium and CO_2. Transport in Porous Media 89(2):265-284.

18. Jung H B, Um W, Cantrell K J (2013) Effect of oxygen co-injected with carbon dioxide on Gothic shale caprock-CO_2-brine interaction during geologic carbon sequestration. Chemical Geology 354:1-14.

19. Kharaka Y K and Maest A S (1992) Water-Rock Interaction. Proceedings of the 7th International Symposium on Water-Rock Interaction. Park City, July 13-18.

20. Kim. J, Kang. Y.T, Choi. C.K (2004) Analysis of convective instability and heat transfer characteristics of nanofluids. Physics of Fluids 16(7):2395–2401.

21. Lasaga, A. C., Soler, J. M., Ganor, J., Burch, T. E., Nagy, K. L. (1994) Chemical weathering rate laws and global geochemical cycles. Geochimica et Cosmochimica Acta 58:(10):2361-2386.

22. Leunissen M E, Blaaderen A V, Hollingsworth A D, et al (2007) Electrostatics at the oil-water interface, stability, and order in emulsions and colloids. Proceedings of the National Academy of Sciences 104(8):2585-2590.
23. Li Jian (2006) Application of Lorentz coefficient to evaluating the macroscopic heterogeneity of reservoir quantitatively taking upper Guantao formation, Chengdao Oilfield as an example. Petroleum Geology and Recovery Efficiency 13(2):24~26.
24. Mangold D C and Tsang C F (1991) A summary of subsurface hydrological and hydro chemical models. Reviews of Geophysics 29(1):51.
25. Nawaz Ahmad, Anders Wörman, Xavier Sanchez-Vila, et al (2016) Injection of CO_2-saturated brine in geological reservoir: A way to enhanced storage safety. International Journal of Greenhouse Gas Control 54:129-144.
26. Palandri, James L. and Yousif K. Kharaka (2004) A Compilation of Rate Parameters of Water-Mineral Interaction Kinetics for Application to Geochemical Modeling. Menlo Park, U.S. Geological Survey, 2004.
27. Plummer L N, Busenberg E (1999) Data on the crystal growth of calcite from calcium bicarbonate solutions at 34 degrees C and CO_2 partial pressures of 0.101, 0.0156 and 0.00102 atmospheres. Journal of Biological Chemistry 272(7):4404-4411.
28. Prigiobbe V, Worthen A J, Johnston K P, et al (2016) Transport of Nanoparticle-Stabilized CO_2 Foam in Porous Media. Transport in Porous Media 111(1):265-285.
29. Ranganathan P, Hemert P V, Rudolph E S J, et al (2011) Numerical modeling of CO_2 mineralisation during storage in deep saline aquifers. Energy Procedia 4(4):4538-4545.
30. Rathnaweera T D, Ranjith P G, Perera M S A, et al (2016) Influence of CO_2-Brine Co-injection on CO_2 Storage Capacity Enhancement in Deep Saline Aquifers: An Experimental Study on Hawkesbury Sandstone Formation. Energy Fuels 30(5):4229-4243.
31. Rosenbauer, R.J., Thomas, B., Bischoff, J.L., Palandre, J. (2012) Carbon sequestration via reaction with basaltic rocks: geochemical modeling and experimental results. Geochimica et Cosmochimica Acta 89: 116-133.
32. Singh H, Hosseini S A, Javadpour F (2012) Enhanced CO_2 Storage In Deep Saline Aquifers by Nanoparticles: Numerical Simulation Results. SPE International Oilfield Nanotechnology Conference & Exhibition. DOI:10.2118/156983-MS
33. Smith J M, Ness V, Abbott M M (2005) Introduction to Chemical Engineering Thermodynamics.
34. Wang S (2018) Shale gas exploitation: Status, problems and prospect. Natural Gas Industry B 5(1):60-74.
35. Ward J. C., Cliffe K. A., Hensen O. E., et al (2014) Dissolution-driven porous-medium convection in the presence of chemical reaction. Journal of Fluid Mechanics 747:316-349.
36. Xu, T., Nicolas Spycher, Sonnenthal, E., Zheng, L, Karsten Pruess (2012) TOUGHREACT User's Guide: A Simulation Program for Non-isothermal Multiphase Reactive Transport in Variably Saturated Geologic Media. Lawrance Berkeley National Laboratory, University of California.

37. Xu, T., Sonnenthal, E., Spycher, N., Zheng, L (2014). A Parallel Simulation Program for Non-Isothermal Multiphase Geochemical Reactive Transport. TOUGHREACT V3.0-OMP Reference Manual. Lawrance Berkeley National Laboratory, University of California.

38. Yang D, Wang S, Zhang Y (2014) Analysis of CO_2 Migration during Nanofluid-Based Supercritical CO_2 Geological Storage in Saline Aquifers. Aerosol and Air Quality Research 14:1411-1417.

39. Yu Miao (2015) A study on fluid-rock interaction after CO_2 flooding in oilfields-Example from southern Songliao Basin. Jilin University, Jilin.

40. Zargartalebi Mohammad, Kharrat Riyaz, Barati Nasim (2015) Enhancement of surfactant flooding performance by the use of silica nanoparticles. Fuel 143 :21-27.

41. Zhan Y, Wan X, Wang Y, He Y (2016) Research progress of nanoparticles in oilfield for oil displacement. Modern Chemical Industry 36(08):37-40.

42. Zhang L, Li D, Ezekiel J, et al (2014) CO_2 geological storage into a lateral aquifer of an offshore gas field in the South China Sea: storage safety and project design. Frontiers of Earth Science 9(2):286-299.

43. Zhang L, Soong Y, Dilmore R M (2016) Investigation on porosity and permeability change of Mount Simon sandstone (Knox County, IN, USA) under geological CO_2 sequestration conditions: a numerical simulation approach. Greenhouse Gases Science & Technology 6(4):546-560.

44. Zhang R, Winterfeld P H, Yin X, et al (2015) Sequentially coupled THMC model for CO_2 geological sequestration into a 2D heterogeneous saline aquifer. Journal of Natural Gas Science and Engineering 27(part_P2):579-615.

Figures

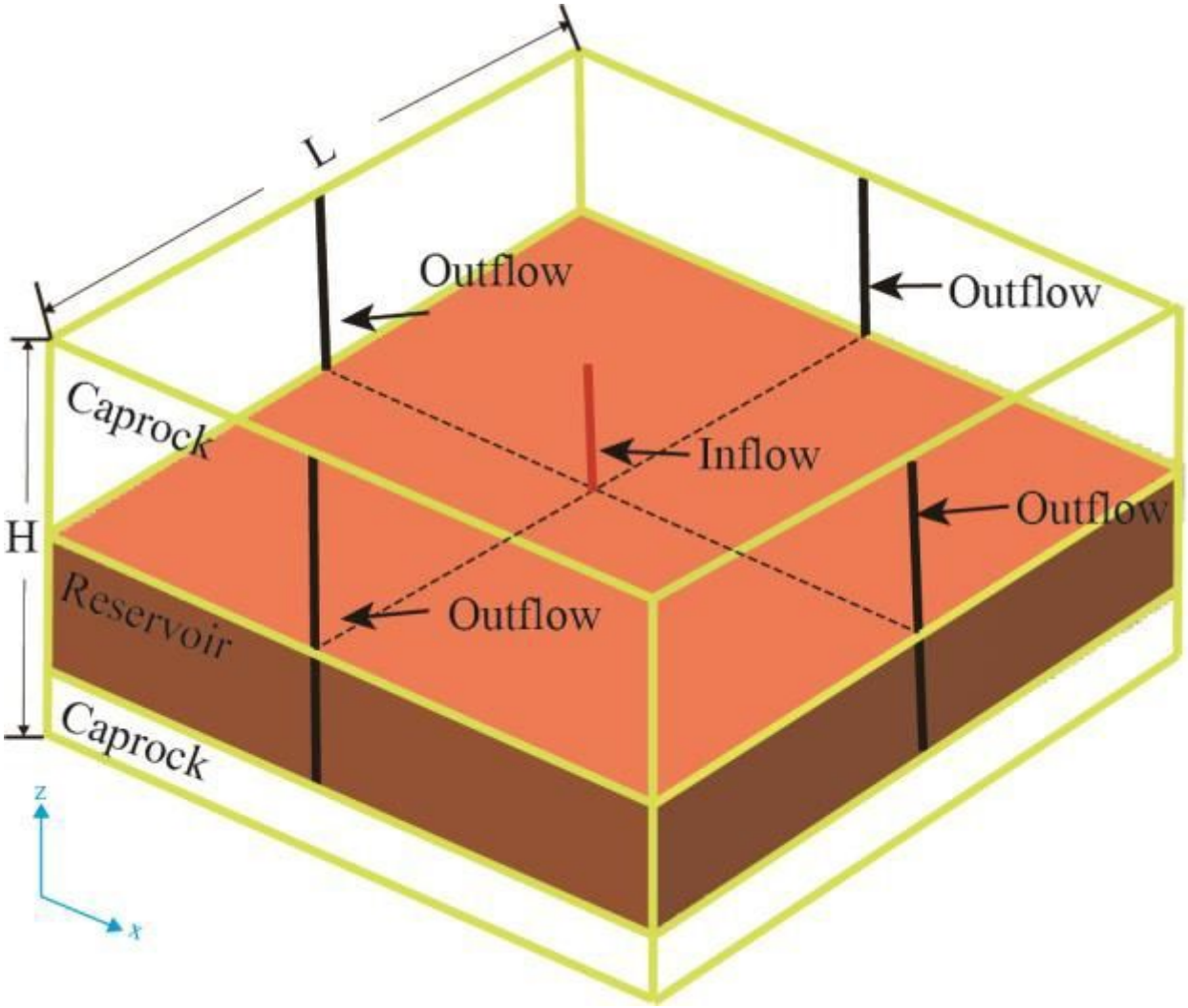

Figure 1

Three-dimensional stratigraphic model

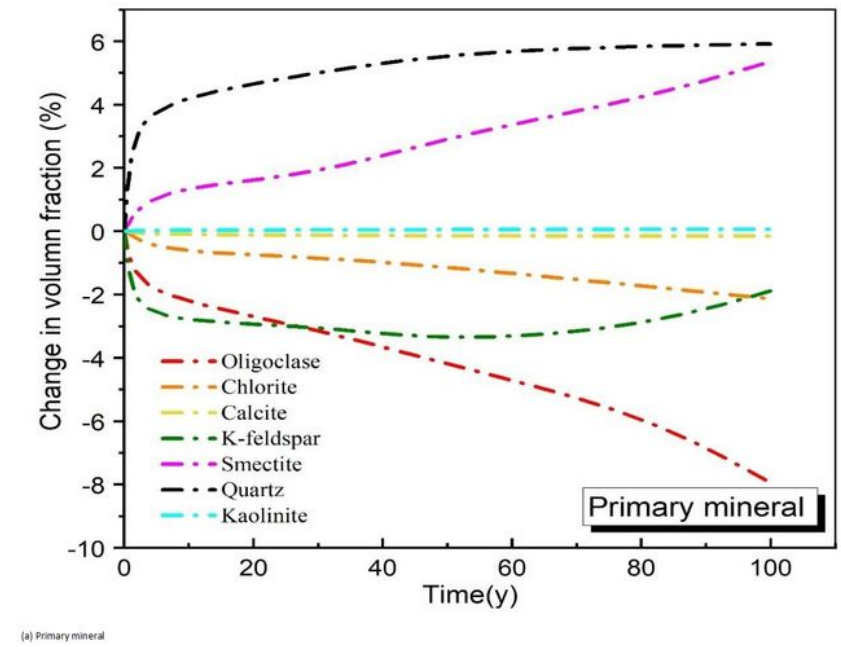

(a) Primary mineral

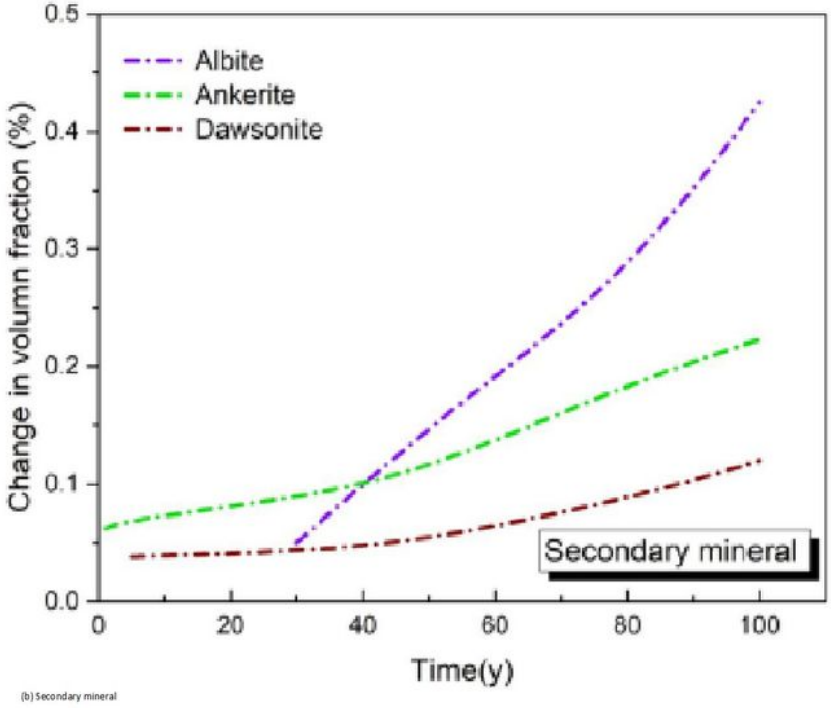

(b) Secondary mineral

Figure 2

Volume fraction changes of minerals

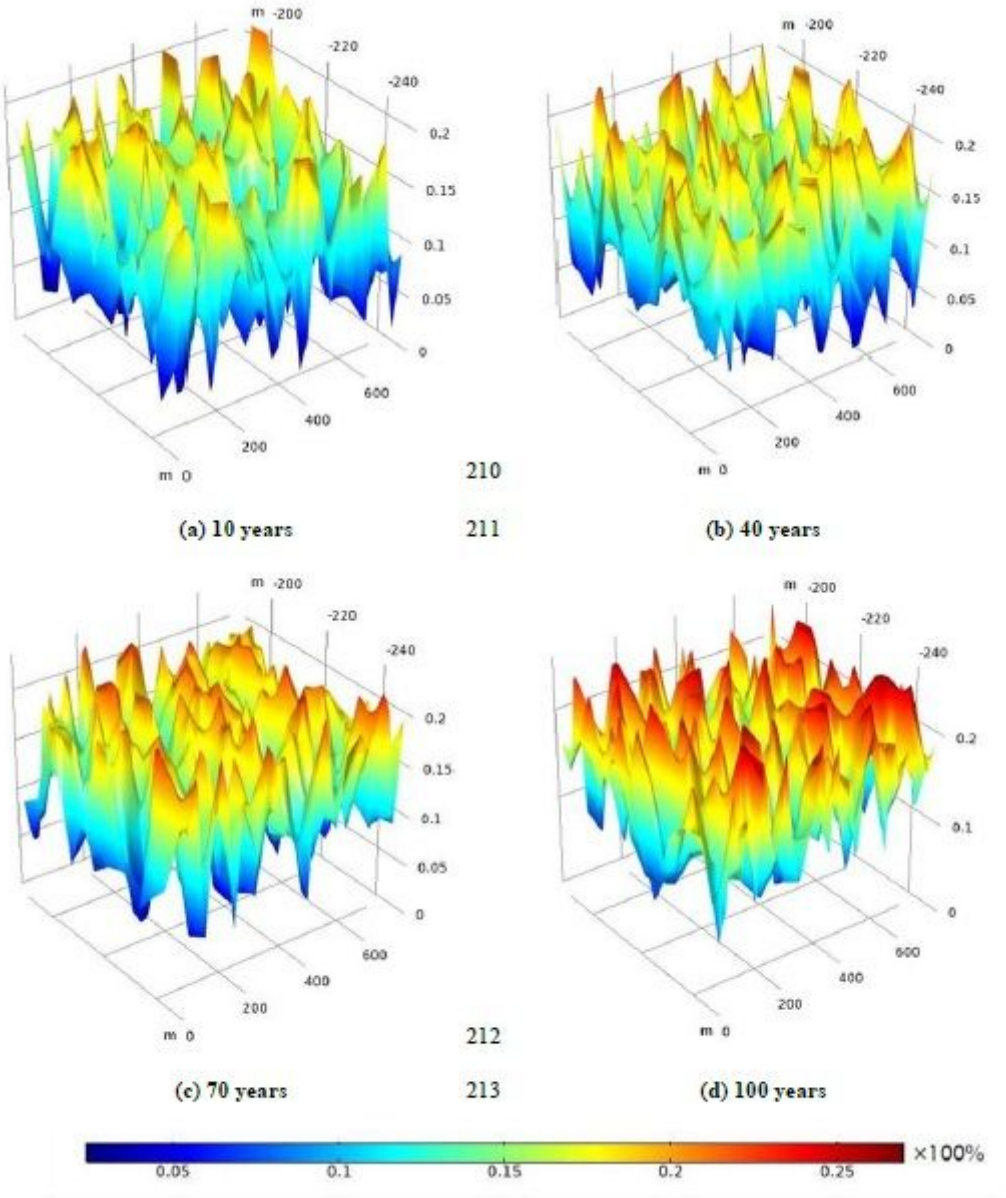

Figure 3

Change of reservoir porosity

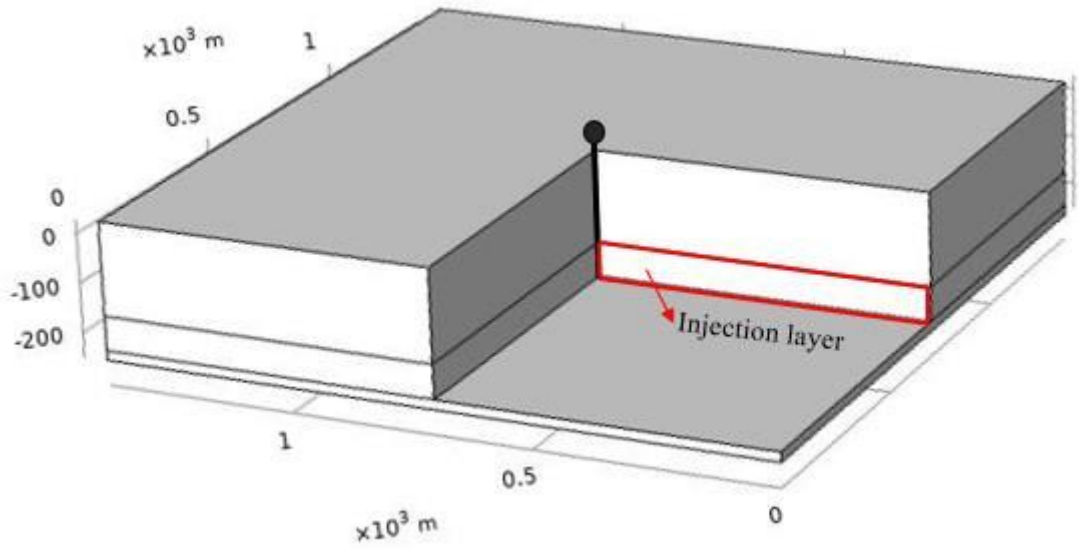

Figure 4

Schematic diagram of injection layer model section

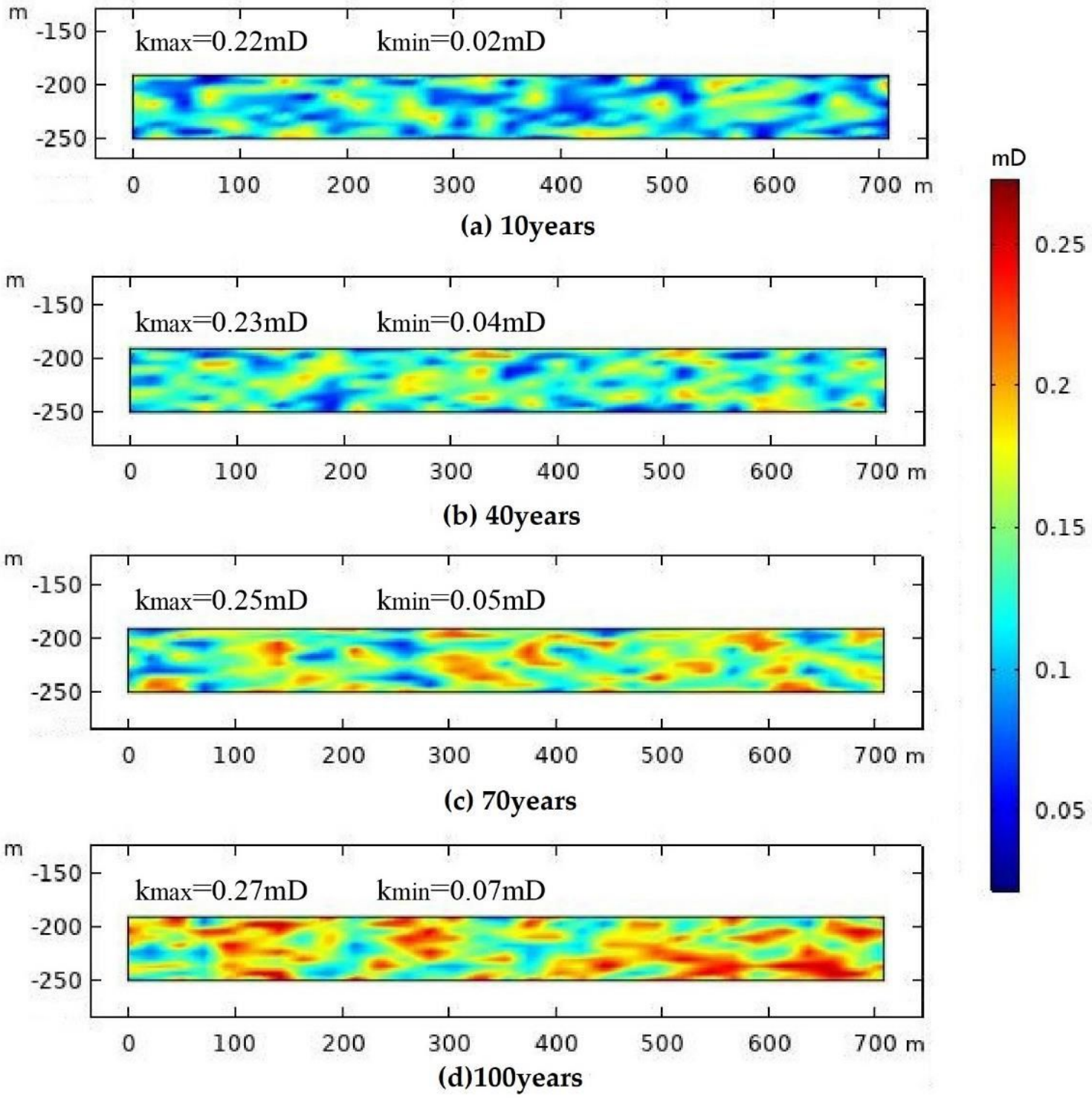

Figure 5

Change of reservoir permeability

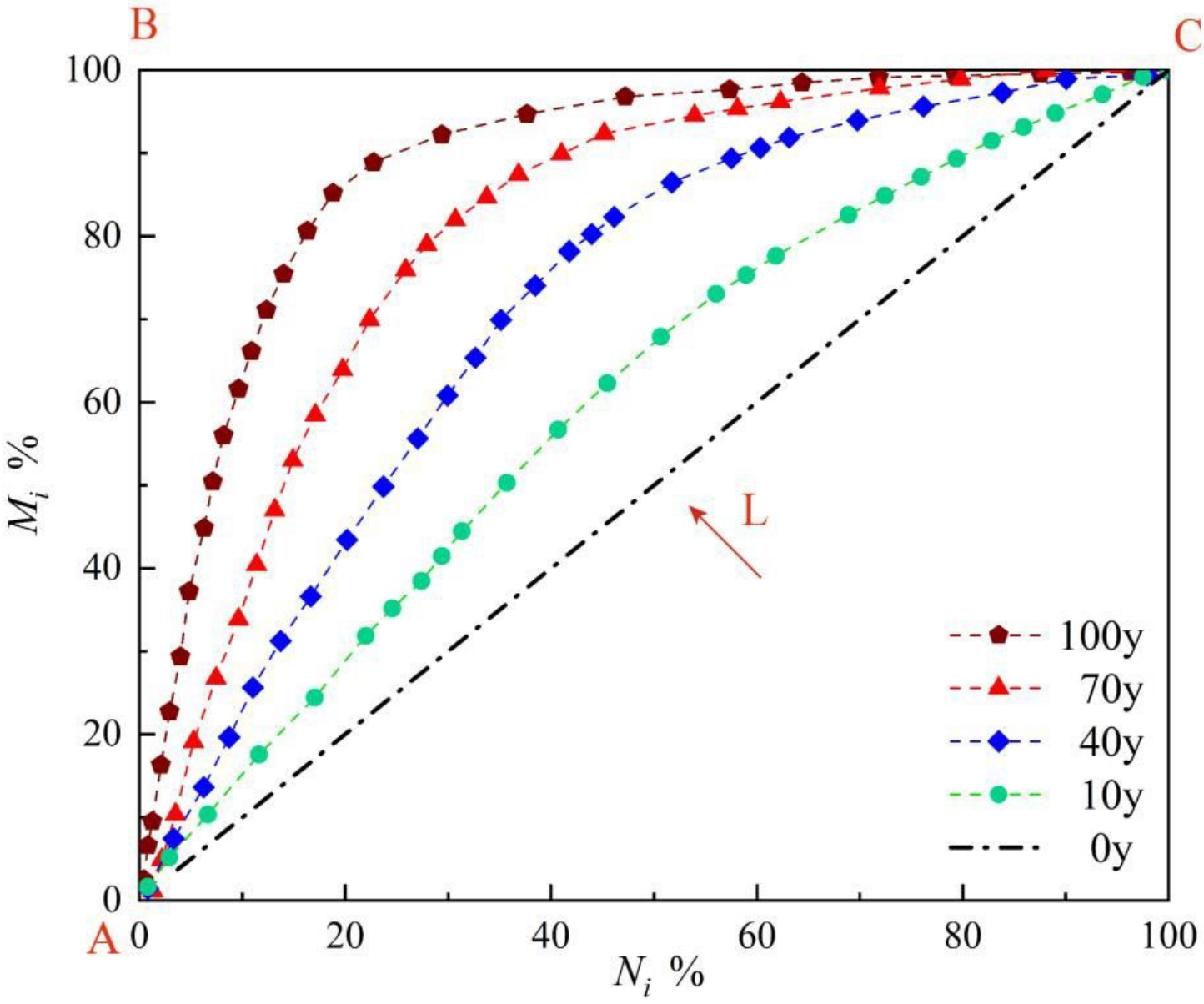

Figure 6

Lorentz curve of rock heterogeneity

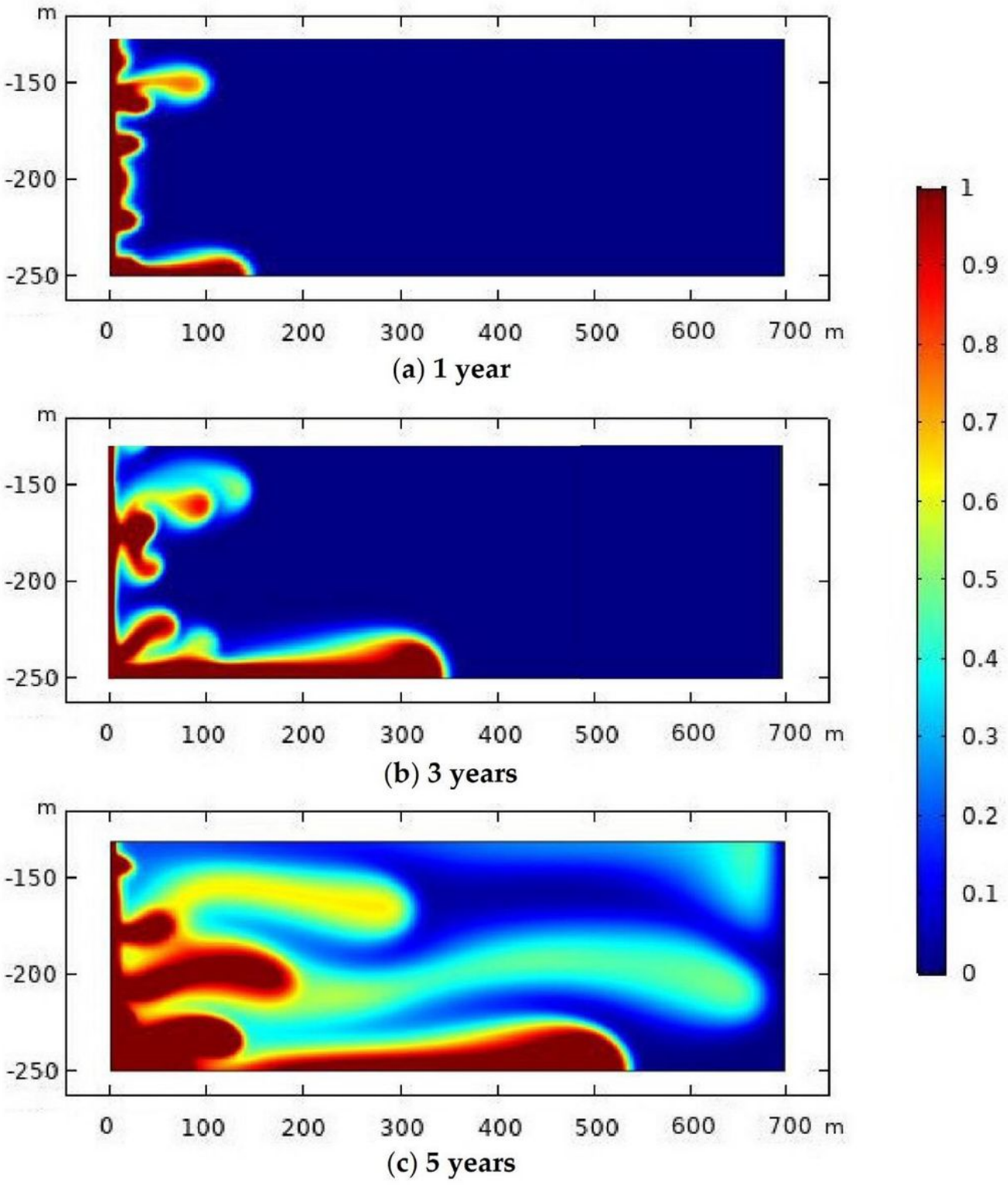

Figure 7

Change of NPs-CO2 saturation after chemical reactions

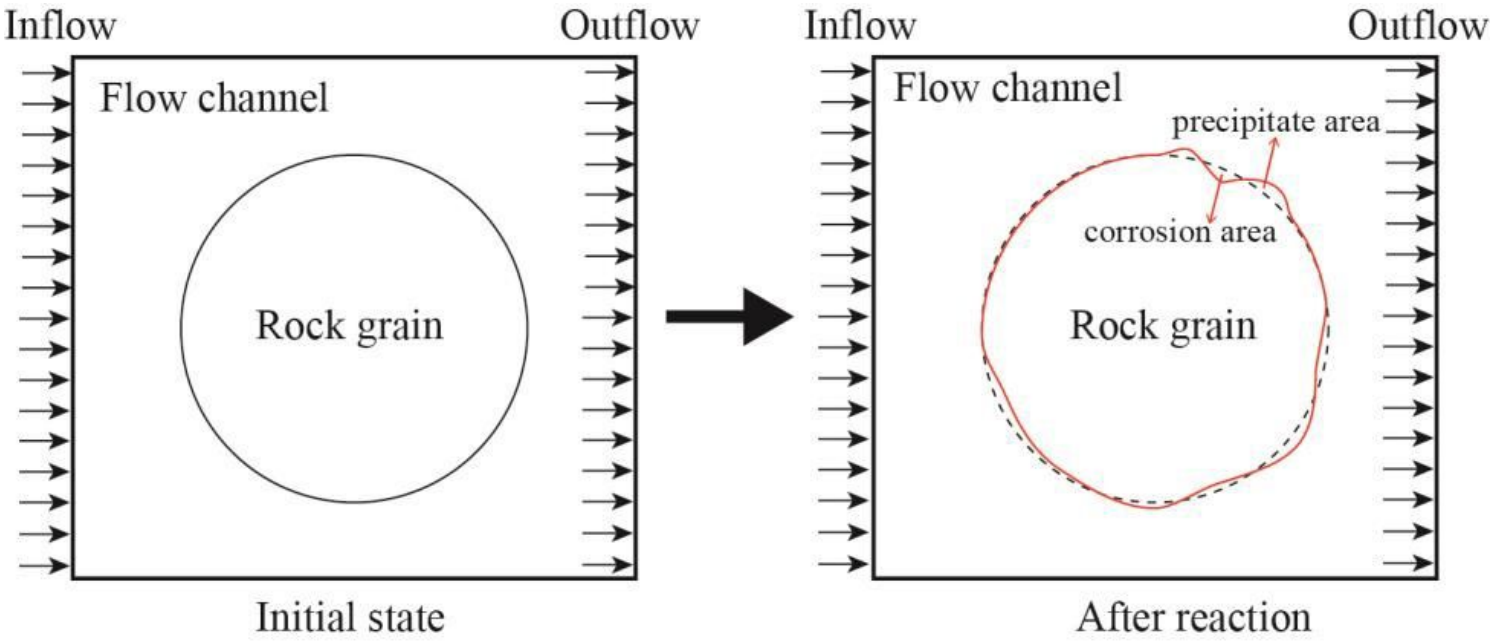

Figure 8

Geometric model after microstructure change

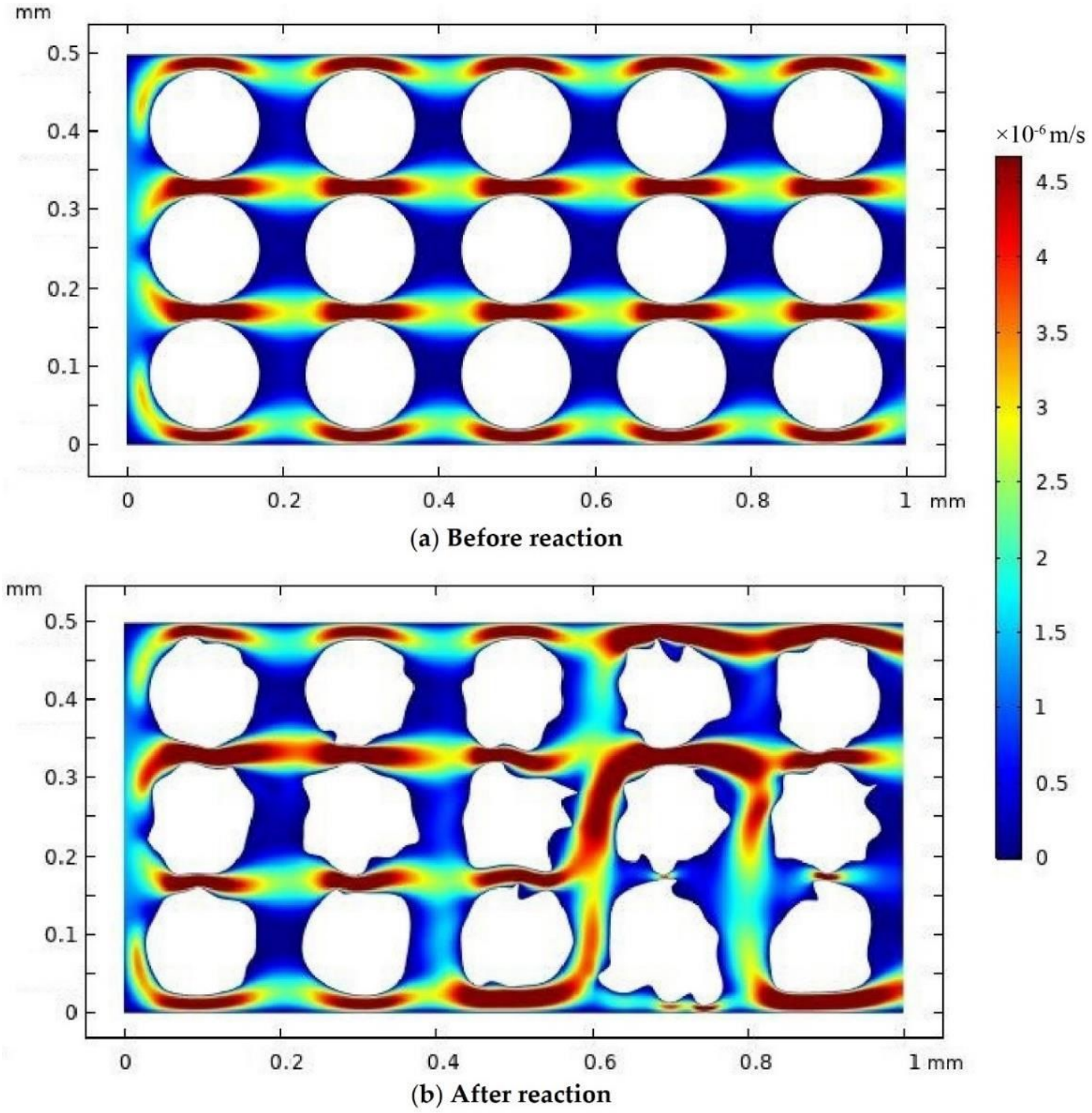

Figure 9

Velocity change of NPs-CO2 flow